

Methodology for the analysis of a novel heat exchanger

Mike Cutbirth

Oklahoma State Univ., Stillwater

Afshin J. Ghajar

Oklahoma State Univ., Stillwater

AIAA, Thermophysics Conference, 31st, New Orleans, LA, June 17-20, 1996

This paper represents a general method for the comparison of hydraulic and thermal performance of different heat exchangers designed for electronic coolant systems. As a case study, the performance of the High Flux Heat Exchanger, HFHE, developed by McDonnell Douglas, is presented. Performance equations for the hydraulic and thermal performance were developed for an applied heat flux as a function of coolant temperature and mass flow rate. In addition, the maximum heat flux capability for the HFHE was determined. The range of coolant temperature for this study was from -10 to 40 C, the range of mass flow rate was from 60 to 240 kg/hr, and the range of applied heat flux was from 0 to 100 W/sq cm. For this study, the coolant polyalphaolefin, PAO, was used. (Author)

METHODOLOGY FOR THE ANALYSIS OF A NOVEL HEAT EXCHANGER

Mike Cutbirth* and Afshin J. Ghajar†
School of Mechanical and Aerospace Engineering
Oklahoma State University, Stillwater, Oklahoma

Abstract

This paper represents a general method for the comparison of hydraulic and thermal performance of different heat exchangers designed for electronic coolant systems. As a case study, the performance of the High Flux Heat Exchanger, HFHE, developed by McDonnell Douglas is presented. Performance equations for the hydraulic and thermal performance were developed for an applied heat flux as a function of coolant temperature and mass flow rate. In addition, the maximum heat flux capability for the HFHE was determined. The range of coolant temperature for this study was from -10 to 40°C, the range of mass flow rate was from 60 to 240 kg/hr, and the range of applied heat flux was from 0 to 100 W/cm². For this study, the coolant polyalphaolefin, PAO, was used.

Nomenclature

A	cross-sectional area of the individual channels of the CHIC, m ²
C	constant relating the Reynolds number and the friction factor for laminar flow
C _n	constants in the curve fit for the pressure, with n=1,2
D	diameter of the individual channels in the CHIC, m
f	friction factor for pipe flow, dimensionless
g	gravitational acceleration, m ² /s
g _c	gravitational constant, kg·m/N·s ²
h _f	total frictional head loss, m
k	thermal conductivity of the HFHE (copper), 300 W/m·°C
k _i	minor loss coefficient for the CHIC for pipe flow, dimensionless
L	length of the individual tubes in the CHICs, m
\dot{m}	mass flow rate of the fluid, kg/hr
p	pressure, psi
Re	Reynolds number (= $\rho V D / \mu$), dimensionless
R	thermal resistance, °C/(W/cm ²)
r _n	distance from CHIC center to symmetry boundary in n-direction, m

Q	volumetric flow rate, m ³ /hr
\dot{Q}	heat transfer, W/cm ² or W per CHIC (each CHIC has a surface area of 1 cm ²)
t	conduction thickness of the target plate, 0.001143 m
T _n	temperature of n, °C (default T is the fluid temperature)
V	velocity of the fluid in the test section, m/s
w _{mech}	mechanical work, J/kg
z	potential energy term, m
Δp	pressure drop across the HFHE, psi
γ	specific weight of the coolant fluid, N/m ³
λ_n	constant in the wall temperature curve fit, n=0,1,2,3
μ	absolute viscosity of the coolant fluid, N·s/m ²
ν	kinematic viscosity of the coolant fluid, m ² /s
ϕ_n	constant in the $\dot{Q}_{loss} / \dot{Q}_{applied}$ curve fit, n=1,...,7
ρ	density of the coolant fluid, kg/m ³
θ_n	constant in the surface temperature curve fit, n=1,2,3
ξ	dummy variable to express the direction of the radial heat flow, cm

Subscripts

c	refers to the case housing of the electronics
f	refers to the coolant fluid
j	refers to the junction of the case housing and the electronic chip
s	refers to the surface of the HFHE
w	refers to the outer wall of the CHIC in the HFHE

Introduction

Modern aircraft have seen an increase in dependence on electronics. Mackowski¹ performed an industrial survey to determine future requirements for the high flux heat removal in advanced electronics systems. The study focused on the technology requirements for military avionics systems. The results of this survey can be sorted into four broad application categories: commercial digital systems, military data processors, power processors and radar and optical systems. The most challenging thermal problems were found to lie with the power controllers. The power controllers contain steady-state heat fluxes reaching at least 100 to 200 W/cm². In addition, pulsed heat loads

* Graduate student, School of Mechanical & Mechanical Engineering.

† Professor, School of Mechanical & Aerospace Engineering.
Associate Fellow AIAA.

of short duration, on the order of a second or less, could exceed 400 W/cm^2 . The heat dissipation of future high-performance data processors was predicted to be somewhat lower, with steady-state levels reaching perhaps 50 to 100 W/cm^2 .

Flynn² made an evaluation of cooling concepts for high power avionics applications. Based on the results of Mackowski¹, a steady-state chip heat flux of 100 W/cm^2 and a maximum chip junction temperature of 90°C was selected as representative thermal requirements for near-future high power avionics components. Several additional constraints were also imposed on the cooler due to the intended application of cooling fighter aircraft electronics. These constraints included a practical lower limit on coolant supply temperature, the preference for a non-toxic, nonflammable, and nonfreezing coolant, the need to minimize weight and volume, and operation in an accelerating environment. Evaluation factors included aircraft system impact, cooler development status, and qualitative assessments of life cycle cost, reliability, maintainability, and safety. Among the emerging cooling technologies, seven concepts were identified which could meet the cooling requirements. The evaluated cooling concepts were: Compact High Intensity Cooler (CHIC), Curved Channel Flow with Subcooled Boiling, Evaporative Spray Cooler, Heat Pipe, Jet Impingement with Subcooled Boiling, Microchannel Cooler, and Pumped Capillary Evaporator. Due to the wide array of cooling techniques, a standard technique for comparison is necessary. Flynn² used the maximum heat flux capability as the one variable for comparison. Using this variable, the Compact High Intensity Cooler (CHIC) concept was selected to meet the demanding thermal requirements foreseen for near-future avionics. However, in the development of the entire coolant loop, not only is the maximum heat flux capability a priority, but also the required pressure drop. Because of the relationship between the mass flow rate and the pressure drop, the minimum flow rate necessary for this maximum heat flux is important. Therefore, the hydraulic performance equation (relating the pressure drop and the mass flow rate) and the thermal performance equation (relating the minimum mass flow rate and the applied heat flux) must be developed.

Case Study: HFHE

For this example case study, the development of hydraulic and thermal performance equations are shown. However, to understand the operating procedure of the selected heat exchanger the background is first presented. The CHIC device was first introduced by Sundstrand in 1983.³ The original CHIC was developed

to provide high intensity (50 W/cm^2) cooling with tight requirements for surface isothermality. This liquid single phase cooler combines the thermal efficiency of multiple jet impingement with a large fin area to produce a high effective heat transfer coefficient.

In the development of the multi-CHIC High Flux Heat Exchanger (HFHE), Flynn et al.⁴ made a comparison of a single jet impingement to multiple jet impingement. Ordinary jet impingement for a single jet can be divided into three zones: the stagnation zone, the turning region and the wall jet region. For jet impingement with multiple jets a fourth region occurs, the jet interaction zone. These four zones can be seen in Fig. 1. The heat transfer rates are high for both of the inner regions. This leads to the conclusion that a multiple number of small jets will be more effective in cooling the same area than a single large jet. Furthermore, the cooling performance can be enhanced by extending the surface areas. Therefore, a greater surface area density per unit volume can be achieved leading to higher fin efficiencies resulting from the shorter conduction path lengths. This is accomplished by using thin lamination plates in close proximity to the heat source being vigorously scrubbed by high heat transfer coolant jets. This maximizing of the surface area and fin effectiveness is in actuality minimizing the thermal resistance. This concept of using multiple jet impingement with the enhancement of multiple plates is the basis for Sundstrand's development of the CHIC.

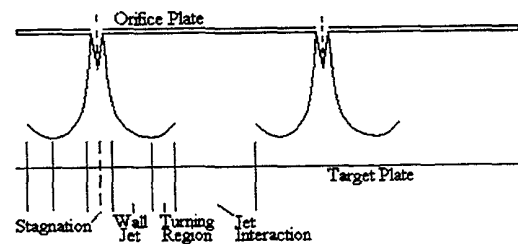


Figure 1. Four characteristic regions for multiple jet impingement heat exchanger.

The operating principle of a CHIC device is relatively simple, as shown in Fig. 2. The liquid enters the inlet port in the end cover, flows through a succession of thin laminates towards the heat acquisition surface, or target plate. The liquid impinges on the target plate, and then is directed back to the drain manifold attached and ultimately to the exit port of the end cover. The electronics device is attached to the opposite side of the target plate. As shown in Fig. 2, the fluid en route to the target plate passes through a jet orifice plate and a spacer plate. The jet orifice plate

usually contains about 50 to 200 small circular holes. In a typical CHIC device, the orifice plate and the spacer plate are repeated several times, with each successive orifice plate acting as a target for the jets from the orifice plate immediately upstream. The orifices are offset by one-half their pitch from plate to plate, so that the liquid impinges on solid metal, then cascades downward as it passes through subsequent orifice plates. The jet interaction of the multiple jets increases the turbulence and mixing, enhancing the heat transfer. Increasing the number of orifice plates, increases the fin area and produces a higher effective heat transfer coefficient. The penalty for a larger number of orifice plates is higher pressure drop and a thicker heat exchanger. Since the 1983 prototype³, several versions of CHICs have been built from copper and aluminum. The devices have been tested with Freon-11³, Freon-113⁵, and water.⁶

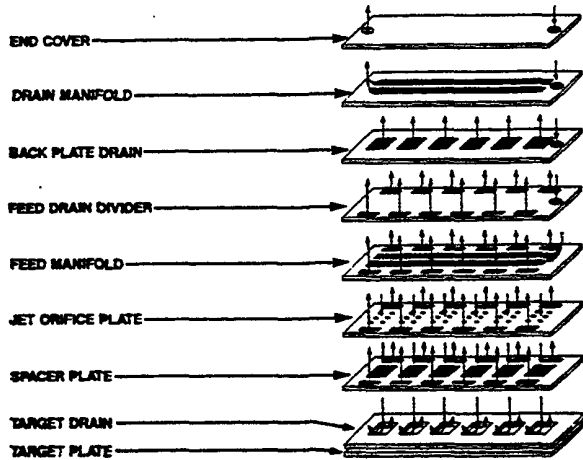


Figure 2. CHIC basic elements and operating principle.⁴

However, this concept only satisfies the requirement for higher heat fluxes caused by modern electronics. To meet the need for an increase in the number of electronic processors, McDonnell Douglas developed the High Flux Heat Exchanger, HFHE. The HFHE consists of 20 CHICs arranged in parallel flow, with each CHIC being 1 cm² and capable of absorbing 100 W/cm². The HFHE was designed to integrate into the Lockhart LOC-E-JECT liquid cooled Navy Standard Electronic Module (SEM-E) used for F-2 avionics cooling. The actual design requirement for the HFHE is the size must fit the SEM-E, approximately 15 by 17 cm, on 1.5 cm pitch, for a total of 200 cm² mounting area per side. Furthermore, the module must absorb 2180 W of steady-state heat load, distributed as 100 W/cm² to 20 cm² of board surface area, consisting of the 20 one cm² CHICs, and 1.0 W/cm² heat flux over the

remaining 180 cm² of surface area. Further details of the high flux heat exchanger design are documented elsewhere.^{4,7}

To ease the process of manufacturing this complex array of CHICs, Sundstrand has developed a process of photo-etching laminae allowing for very accurate location of the orifices on the plates.⁷ The laminae are then stacked and bonded. Diffusion bonding was used for the copper boards and vacuum brazing was used for the aluminum boards. This photo-etching process allows virtually anything that can be drawn to be fabricated.

Because of this need for liquid cooling to absorb higher heat fluxes, additional considerations must be introduced. With the added intermediate aircraft cooling loop associated with liquid cooling, leaking and handling create a selection process for the liquid coolants. And with the increase of emphasis on safety and environmental, this liquid coolant must be non-toxic, non-corrosive, and be an adequate dielectric. In the past, silicate-ester based fluids, Coolanol 25R, were widely used as the liquid coolant in military avionics systems. These fluids have caused significant and sometimes catastrophic problems due to their hygroscopic nature and subsequent formation of flammable alcohols and silica gel. The alcohol by-product lowers the fluid flashpoint, increasing the risk of aircraft fires. The gelatinous precipitate called the "black plague", deposits on the surfaces of the electronics components, causing avionics equipment to malfunction. In order to solve the problems associated with Coolanol, the Air Force and the Navy investigated the possibility of direct replacement of silicate-ester based fluids with hydrogenated polyalphaolefin based fluids. Their studies concluded that polyalphaolefin (PAO) fluids are chemically more stable, (do not hydrolyze to form either silica gel or alcohol by-products), less costly, offer equal or improved dielectric characteristics, and meet or exceed military requirements for a dielectric coolant.^{8,9} Due to these desirable properties of PAO, the Air Force and the Navy, for some selected fighter aircraft, have both replaced the liquid coolant, Coolanol, used in their fighter aircraft electronic cooling systems with PAO.

In a recent study,¹⁰ the hydraulic and thermal performance of PAO and Coolanol 25R in different flow regimes, laminar and turbulent, were compared. The results indicated that at normal operating temperatures the two coolants were reasonably close and fairly independent of the flow regime. However, at low temperatures, dependent on the flow regime, there could be substantial difference between the hydraulic and thermal performance of the two fluids. Particularly, at

temperatures below 0°C, PAO's hydraulic performance in the laminar flow region, and its thermal performance in the turbulent flow region, are inferior to those of Coolanol 25R at comparable conditions.

Coolanol has been a standard coolant of fighter aircraft, but is currently being phased out by PAO, which is much less prone to decomposition. Therefore, in this study of the performance for the High Flux Heat Exchanger, PAO was selected as the liquid coolant.

The specific objectives of this study are to investigate the influence of the coolant flow rate and temperature on the pressure drop across the inlet and outlet of the HFHE, to investigate the influence of the coolant flow rate and temperature on the heat flux removal capabilities of the HFHE for steady state heat loads, and to develop a guideline for the performance of the HFHE. This will consist of a performance chart with the necessary coolant flow rate with respect to the coolant temperature to achieve the 100 Watts of heat flux removal and the corresponding charts for the pressure drop for the performance flow rate and temperature.

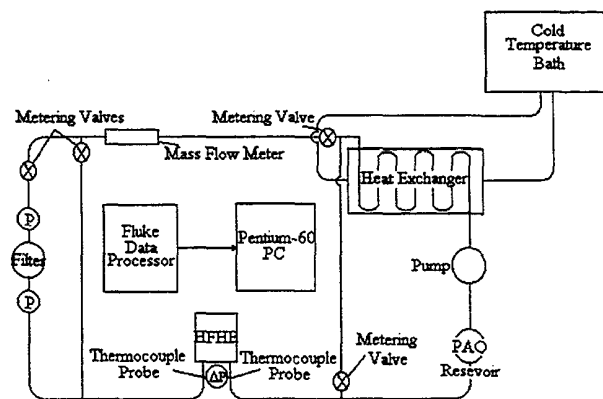


Figure 3. Schematic diagram of the experimental setup.

Experimental Setup

To conduct the hydraulic and thermal tests necessary for the performance equations a test loop, shown in Fig. 3, was constructed. A two liter reservoir houses the liquid coolant, PAO. The coolant is then pumped, by a constant volume gear pump powered by a variable speed DC motor through a magnetic coupling, to the in-loop heat exchanger. The pump-motor is capable of producing flow rates from 30 to over 255 kg/hr. Because of the need for a constant coolant temperature, this in-loop shell and tube heat exchanger in conjunction with an outside cold temperature bath was necessary. This constant temperature bath consisted

of an FTS Systems RC-50 recirculating cooler with FTS Systems HT-30 as the heat transfer fluid. The RC-50 had both a cooling mode and a heating mode, allowing control of the coolant temperature well beyond the temperature range for these tests. Downstream of the in-loop heat exchanger in the test loop is the flow meter. The flow meter consisted of a Micromotion DS25 mass flow meter that had an output of 4 to 24 mA. This output correlated to a flow rate of 0 to 4.32 kg/min. This flow meter was calibrated using the bucket and stopwatch technique, with the output being a linear calibration, ($\dot{m} = 0.2406 \text{ mA} - 0.9635$), with an uncertainty of $\pm 0.10 \text{ kg/min}$.

After the flow meter, the fluid passes through a 20-micron filter. This filter, made by HYCON, was used to remove particulates that could clog the small coolant passages in the HFHE. To monitor the performance of the filter, two analog pressure gauges were placed on the filter inlet and outlet. A high pressure drop reading from the gauges would indicate that the filter needed to be replaced. After any particulates in the fluid have been removed, the coolant enters the test section (HFHE). One quarter inch pressure taps were made immediately upstream of the inlet of the HFHE and immediately downstream of the outlet. The pressure taps were connected to a Validyne P305D-50 differential pressure transducer with quarter inch vinyl tubing. The differential pressure transducer was calibrated over the range of 0-125 psi. Because of the large pressure range, the calibration process itself consisted of a combination of two techniques. For the lower range, 0-50 psi, the transducer was calibrated using a 60-0-60 inch U-tube mercury manometer. For the upper range 50-125 psi, the transducer was calibrated using a dead weight tester. The combination of these two techniques produced a linear curve ($\Delta p = 14.3627 \text{ Voltage} - 6.7044$) with a corresponding uncertainty of $\pm 0.05 \text{ psi}$.

The thermocouples are the last data generating components of the test loop. The thermocouples consisted of numerous 30-gauge Omega T-type thermocouples and two 1/8 inch Cole Parmer T-type temperature probes. To calibrate the thermocouples a constant temperature bath in conjunction with an OMEGA platinum-80 temperature sensor were used. The calibration range covered -20 to 60°C with an interval of 10°C. A typical calibration curve consisted of a linear curve with an uncertainty of $\pm 0.1^\circ\text{C}$ (thermocouple 15: $T_{\text{act}} = 1.0009 T_{\text{meas}} - 0.6048$). The temperature probes were placed at the same location in a cross fitting as the pressure taps to give the inlet coolant temperature and the outlet coolant temperature of the HFHE. Furthermore, the individual thermocouples were placed on the surface of the HFHE to generate

temperature curves used to develop the equations for the radial heat loss due to conduction from the surrounding CHIC needed for this case study (discussed in the Thermal Performance section). The placement of these thermocouples is shown in Fig. 4.

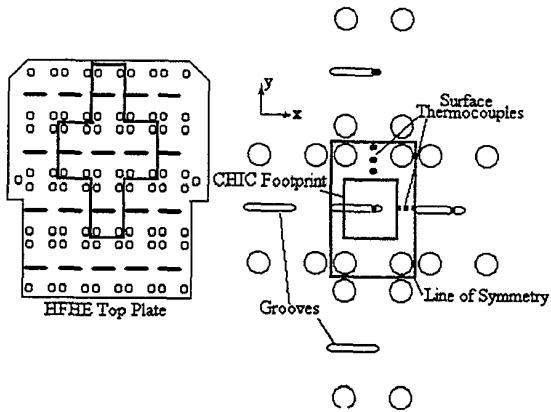


Figure 4. Placement of the surface thermocouples.

Also shown in Fig. 4 are the grooves made in the target plate of the HFHE. These grooves allowed for the placement of a thermocouple capable of measuring the wall temperature of the HFHE under operating conditions. These grooves consisted of a channel cut of 0.05 cm in depth across the middle of the target plate for each CHIC. Each component was connected by 0.5 inch I.D. stainless steel tubing and Swedgelock compression fittings.

The heat source for the thermal tests provided some difficulty because of the high heat fluxes, $100\text{W}/\text{cm}^2$, necessary. Very few dependable heaters are capable of this high heat flux. Therefore, a heat flux amplifier, similar to the one used by Grote et al.,⁶ was added to the test setup. The details of this particular heat flux amplifier, is given by McDonnell Douglas via Wright Laboratories.⁴ Simply, this copper amplifier reduces the heat conduction area from 40.3 cm^2 where the heaters are mounted, to 1.0 cm^2 where the heat is transferred to the HFHE. Thus, low heat flux heating elements ($2.5\text{ W}/\text{cm}^2$) at the top of the amplifier can produce a high heat flux ($100\text{ W}/\text{cm}^2$) at the amplifier/HFHE interface. The actual heat source consisted of a Minco mica circular heater with a radius of 2 inches and a resistance of 19 ohms. This heat source is capable of producing heat fluxes, that in conjunction with the amplifier, exceed the $100\text{ W}/\text{cm}^2$ guideline used in this case study. The lower 1.3 cm of the amplifier has a constant area of one cm^2 . In this section, there are three parallel planes of thermocouples spaced 0.25 cm apart. Nine T-type thermocouples are placed at each of the three planes. The temperature at the amplifier/HFHE interface can be approximated by projecting the temperatures in the three planes of the amplifier by using a linear least squares fit.

This approximation is used to indicate if the thermocouple placed in the groove is accurate. The thermocouples in the amplifier were calibrated using the same technique as the surface thermocouples and the temperature probes.

To monitor the heater inputs, thermocouples, differential pressure transducer, flow meter, and the heater inputs, a Fluke data processor was used. The Fluke data programming consists of all of the calibration curves with the output being a DOS data file. A custom data reduction program was then used to generate the final reduced data.

Hydraulic Performance Equation

The first step in the process of comparison between heat exchangers is the development of an expression relating the dynamic pressure drop across the heat exchanger and the mass flow rate. This process is illustrated through the case study of the High Flux Heat Exchanger and the coolant PAO. The data set used to construct the hydraulic expression consisted of pressure drop measurements across the HFHE while varying the mass flow rate between 60 and 240 kg/hr by 15 kg/hr and the coolant temperature between -10 and 50°C by 10°C . In addition, because of the emphasis on low temperature measurements for system start up the -15°C was also included. This dynamic pressure was measured directly with a pressure tap immediately before and after the inlet and outlet, respectively. Figure 5 shows the family of curves representing the results of these tests. The next step in the methodology for the comparison of the various heat exchangers is to develop an analytical equation corresponding to the experimental results. For this particular heat exchanger, an orifice-tube model.

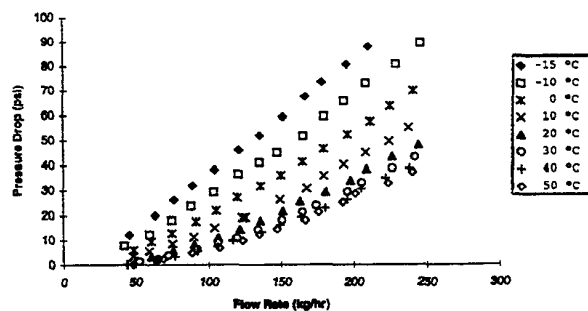


Figure 5. Pressure drop measurements for the HFHE.

To construct this orifice-tube model, first begin with the steady-state incompressible flow energy equation for a control volume in a pipe with several inlet and exit stations. This is shown by Eq. (1).

$$w_{\text{mech}} = \sum_e \left(\frac{p}{\gamma} + \frac{V^2}{2g} + z \right)_e - \sum_i \left(\frac{p}{\gamma} + \frac{V^2}{2g} + z \right)_i + h_f \quad (1)$$

However, Eq. (1) can be simplified by considering the entire HFHE as the control volume. This translates to one inlet and one exit. In addition, the friction head loss, h_f , can be expressed by a viscous-frictional loss term and a dynamic (minor) loss term. Therefore, the energy equation can be expressed in its final form.

$$\left(\frac{p}{\gamma} + z + \frac{V^2}{2g}\right)_1 + (\sum k_i)_{\text{minor}} = \left(\frac{p}{\gamma} + z + \frac{V^2}{2g}\right)_2 + f \frac{L V^2}{D 2g} + \sum k_i \frac{V^2}{2g} \quad (2)$$

Equation (2) can be further modified by the following assumptions: the HFHE is located in a horizontal plane, the tests were performed for an isothermal condition, and both the viscous-friction term and the dynamic term can be modeled by a summation of the individual viscous-friction terms and dynamic terms associated with the individual plates in each CHIC. These assumptions translates to the change of potential energy, $z_1 - z_2$, to be negligible. In addition because the temperature for each individual test was held constant, the density can be considered as a constant. Applying this with the realization that the inlet and outlet of the HFHE contain the same cross-sectional area, the velocities of the inlet and the outlet must also be equivalent. Therefore, the change of kinetic energy, $(V^2/2)_1 - (V^2/2)_2$, is also negligible. Applying these modifications to Eq. (2) yields the equivalent orifice-tube model which can be expressed as:

$$\Delta p = \sum_{i=1}^n k_i \frac{V_i^2 \rho}{2g_c} + \sum_{i=1}^n f_i \frac{L_i}{D_i} \frac{\rho V_i^2}{2g_c} \quad (3)$$

If a check on the flow regime is performed, the maximum Reynolds number, occurring at a mass flow rate of 240 kg/hr and a coolant temperature of 50°C, at the inlet/outlet of the HFHE (pipe diameter of 1.27 cm) is 2149. Furthermore, if the Reynolds number is calculated at the other extreme of the ranges, a mass flow rate of 60 kg/hr and a coolant temperature of -10°C, the value is 50. Therefore, the Reynolds number at the inlet and outlet of the HFHE over the entire flow rate range and coolant temperature range is predominately laminar. Furthermore, although the individual tubes in the HFHE are much smaller than the inlet/outlet pipe, the flow rate through each CHIC is only 1/20 the flow rate through the inlet/outlet pipe and the flow rate through each individual jet is 1/1200 (three rows of twenty jets in each CHIC) of the flow rate through the inlet/outlet pipe. Some turbulence does occur through the abrupt turning of the flow through downstream orifice plates in the CHICs. However, the increased pressure drop due to this turbulence is modeled in the dynamic pressure loss term, k_i . Therefore, the assumption that the flow is predominately

laminar is valid and the friction factor can be expressed as:

$$f = \frac{C}{Re} = \frac{C\mu}{\rho V D} \quad (4)$$

Using this expression for the friction factor and the expression that the velocity is equal to the volumetric flow rate divided by the cross-sectional area, $V=Q/A$, and substituting into Eq. (3) yields the following equation for the pressure drop across the HFHE:

$$\Delta p = \sum_{i=1}^n \rho Q^2 \left(\frac{k_i}{2A_i^2 g_c} \right) + \sum_{i=1}^n \mu Q \left(\frac{CL_i}{2g_c A_i D_i^2} \right) \quad (5)$$

Noticing that the terms in the parentheses, the minor loss coefficient of each individual passage, the cross-sectional area of the individual passages, the gravitational constant, the length of the individual passages, the diameter of the individual passages, and the constant relating the Reynolds number and the friction factor, are independent of the flow rate and the coolant temperature, these terms can be replaced by constants. These constants are shown in Eq. (6).

$$\Delta p = C_1 \mu Q + C_2 \rho Q^2 \quad (6)$$

Because the data set used in this case study consisted of mass flow rates, a simplification of Eq. (6) can be made using the expression that the volumetric flow rate, Q , is equivalent to the mass flow rate, \dot{m} , divided by the density, ρ . Using this expression, the final equation for the pressure drop across the HFHE can be shown as:

$$\Delta p = \frac{(C_1 \mu \dot{m} + C_2 \dot{m}^2)}{\rho} \quad (7)$$

Equation (7) equates the pressure drop across the HFHE with a function of the viscosity, density, and the mass flow rate. However, the viscosity and density are inert properties of the coolant PAO and are strongly temperature dependent. Therefore, Eq. (7) actually indicates that the pressure drop across the HFHE is a function of the mass flow rate, type of coolant, and the coolant temperature. To complete this transition from viscosity and density to the coolant type and temperature, equation for the density and viscosity must be constructed. These equations were developed by Ghajar et al.,¹¹ and shown below. First, the viscosity of the PAO follows the following equation:

$$\nu = \left(10^{\left(\frac{10^{9.67}}{T^{3.928}} \right)} - 0.70 \right) \times 10^{-6} \quad (8)$$

In addition, the density of the coolant fluid PAO is given by the following equation:

$$\rho = 136 \times 10^3 - 4.56T + 0.01577T^2 - 0.280 \times 10^{-4}T^3 + 0.174 \times 10^{-7}T^4 \quad (9)$$

For both Eqs. (8) and (9), the coolant temperature was in K while the viscosity was in m^2/s and the density was in kg/m^3 . Completing the transition by substituting the expressions for the viscosity and density into Eq. (7), with the realization that the kinematic viscosity is equal to the absolute viscosity divided by the density, the final equation for the pressure drop across the heat exchanger was created.

$$\Delta p = C_1 \left[\left(10^{\left(\frac{10^{0.47}}{T^{0.333}} \right)} - 0.70 \right) \times 10^{-6} \right] \dot{m} \quad (10)$$

$$+ C_2 \frac{\dot{m}^2}{(136 \times 10^3 - 4.56T + 0.01577T^2 - 0.28 \times 10^{-4}T^3 + 0.174 \times 10^{-7}T^4)}$$

With units for the pressure drop to be psi, the mass flow rate to be kg/hr, and the coolant temperature to be K, the constants for C_1 and C_2 were determined to be 7354.83 and 0.43, respectively, for all of the inlet coolant temperatures. These constants yield an expression for the pressure drop that fits the experimental data at each discrete temperature with a standard deviation of 1.8 psi. In addition the equation contains a maximum error of 3.5 psi at a coolant temperature of $-15^\circ C$ and flow rate of 180 kg/hr. This model, as shown in Fig. 6, fits the data well, especially at medium and high flows. The form of the equation of this model is constrained to pass through the origin. This may affect the fit at the low flow conditions.

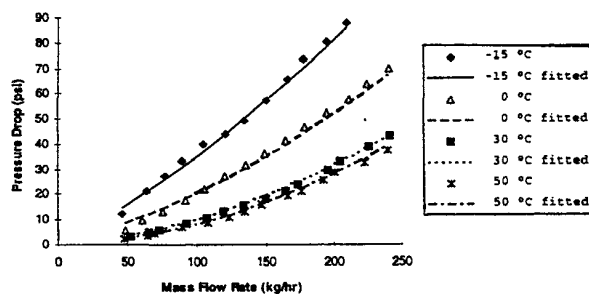


Figure 6. Curve fit for the pressure drop data.

Although this hydraulic performance equation is unique for the HFHE, the procedure for the development of the hydraulic performance equation can be simulated for the various electronic cooling heat exchangers. Possible differences occur in that the coolant PAO has unique density and viscosity characteristics and the flow regime for the HFHE remained laminar. In addition, some heat exchangers cannot use the orifice-tube model

(such as the evaporative spray cooler). However, some form of Eq. (10) in which the pressure drop across the heat exchangers is a function of the coolant temperature and the mass flow rate should be possible.

Thermal Performance Equation

The hydraulic performance equation relates the pressure drop to the mass flow rate. To relate the mass flow rate to the applied heat flux, a thermal performance equation must be developed. For the case study of the HFHE, a data set was created to construct this thermal performance equation. The data set consisted of measuring various temperatures on the HFHE and the heater while varying the mass flow rate from 60 to 240 kg/hr, the coolant temperature from -10 to $40^\circ C$, and the applied heat load from 20 to $100 W/cm^2$. Because the HFHE was designed to not only remove the higher heat fluxes of future electronic components but also to handle the increased number of these electronic components, the HFHE consists of twenty parallel CHICs. Therefore, to create the thermal performance equation for this case study, an assumption that all CHICs are identically independent was made, and a heat load was applied to only one of the CHICs at a time. With this simplification, a correctable error occurs due to the layout of the CHICs in the HFHE. In the layout, each CHIC is surrounded by other CHICs that have zero heat flux being applied. This translates to conductive heat transfer radially through the HFHE from the CHIC being tested to the surrounding CHICs, thereby causing the actual heat flux absorbed by the CHIC to be less than the heat flux applied. So, for this case study an intermediate step was added to the development of the thermal performance equation. This step included constructing two-dimensional heat transfer model by taking temperature measurements surrounding the tested CHIC. Figure 4 shows the placement of these surface thermocouples. This temperature was then plotted and an exponential decaying curve was fitted. This curve fit followed the following equation:

$$T_s = \theta_1 + \theta_2 e^{-\theta_3 \xi} \quad (11)$$

Where the variable ξ is a dummy variable representing the distance from the edge of the CHIC in the x or y direction. The constants θ are determined by the curve fit and are dependent on the heat load, fluid temperature, flow rate, and CHIC location. The equation is then differentiated and evaluated at the ξ value representing the symmetry line, shown in Fig. 4. From this temperature gradient, the heat conducted across the line of symmetry in the x or y direction can be approximated from the following equations, respectively:

$$\dot{Q}_{+/-x} = \pi k r_x t \frac{dT_x}{dx} \quad (12)$$

$$\dot{Q}_{+/-y} = \pi k r_y t \frac{dT_y}{dy}$$

The final equation in this intermediate step is to develop an equation that yields the conductive heat loss in the radial direction as a function of the mass flow rate, the coolant temperature, and the applied heat flux. To complete this, the reduced experimental data using Eq. (12), was fitted with a curve that was expressed as the following:

$$\frac{\dot{Q}_{\text{loss}}}{\dot{Q}_{\text{applied}}} = \phi_1 + (\phi_2 + \phi_3 e^{(\phi_4 T)}) e^{((\phi_5 + \phi_6 e^{(\phi_7 T)})^m)} \quad (13)$$

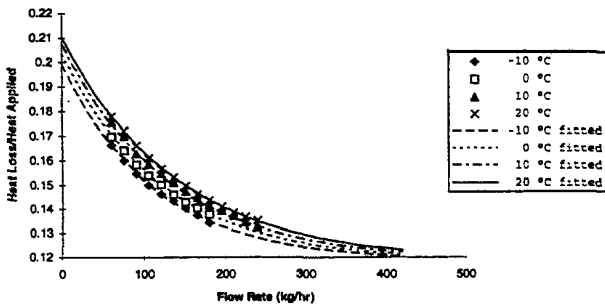


Figure 7. Radial heat loss due to conduction heat transfer for an applied heat load of 100 W.

However, the constants ϕ_n are dependent on the applied heat load. Typical values for these constants can be seen for the applied heat flux of 100 W/cm²: ϕ_1 (0.11858), ϕ_2 (0.11897), ϕ_3 (-0.7860), ϕ_4 (-0.011485), ϕ_5 (-0.0046646), ϕ_6 (-0.37727), and ϕ_7 (-0.017087). In addition, a typical curve fit can be seen for the case of an applied heat flux of 100 W/cm² in Fig. 7. This equation fits the experimental data with a standard deviation of 0.00053 and a maximum error of 0.0015.

After this intermediate step for correcting the error caused by using one CHIC at a time was completed, the actual thermal performance equation could be constructed. The first step in the thermal performance analysis is to develop a thermal resistance equation for the HFHE. To accomplish this, an analytical model must be developed for the wall temperature of the HFHE. This wall temperature theoretically should be a linear function of the heat flux, as shown below:

$$T_w - T_f = \psi \dot{Q} \quad (14)$$

However, for this case study the cooling method is jet impingement. In a jet impingement heat exchanger, the efficiency of the heat exchanger is dependent on the flow rate. Therefore, the resulting equation for the wall temperature should be a combination of a linear function of the heat flux with the constant, ψ , for the heat flux to be exponentially dependent on the flow rate. Because in this case study, only one heat load was applied to the heat exchanger, the heat load in Eq. (14) must be the net heat load. However, when heat loads are applied to all of the CHICs located in the HFHE simultaneously, the net heat load will approach the applied heat loads. Using the experimental data collected during the case study, the equation for the wall temperature for the HFHE was given by the following equation:

$$T_w - T_f = \lambda_0 + (\lambda_1 + \lambda_2 e^{(\lambda_3 \dot{Q})}) \dot{Q} \quad (15)$$

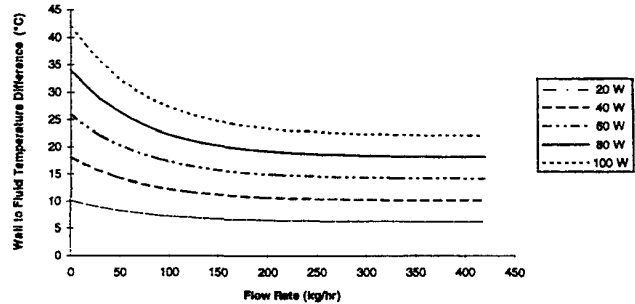


Figure 8. Wall temperature as a function of the flow rate.

The constants λ_n are independent of the flow rate, heat load, and fluid temperature and have the following values: λ_0 (2.25), λ_1 (0.19779), λ_2 (0.19968), and λ_3 (-0.013115). This curve fit, shown in Fig. 8, produces a standard deviation of 0.28°C and a maximum error of 0.71°C. Now defining the thermal resistance of the HFHE as the difference between the wall and fluid temperatures divided by the heat flux, shown in Eq. (16) we can substitute Eq. (15) for the wall temperature.

$$R_{wf} = \frac{T_w - T_f}{\dot{Q}} \quad (16)$$

This substitution results in the final equation for the thermal resistance of the HFHE, shown in Eq. (17).

$$R_{wf} = \frac{2.25 + (0.20 + 0.20 e^{(-0.013 \dot{Q})}) \dot{Q}}{\dot{Q}} \quad (17)$$

One criteria for these heat exchangers is that the junction temperature must be retained at 90°C. Therefore, the thermal resistance between the wall of the heat exchanger and the junction must be included in Eq.

(16). Rearranging Eq. (16) for the heat flux, with the addition of these thermal resistances yields Eq. (18).

$$\dot{Q} = \frac{T_j - T_f}{R_{jc} + R_{cw} + R_{wf}} \quad (18)$$

The thermal resistances shown in Eq. (18) represent the thermal resistance between the junction and the case interface and the thermal resistance between the case interface and the wall of the HFHE. The location of these thermal resistances, the fluid temperature, and the junction temperature are shown in Fig. 9. McDonnell Douglas⁴ assumed the values of these thermal resistances both to be 0.2°C/(W/cm²). Using these thermal resistances to be typical values, the heat flux becomes a function of the fluid temperature, mass flow rate, and the heat load. Therefore, Eq. (18) reduces to a function of the fluid temperature, mass flow rate, and the heat load. Therefore, if Eq. (17) is substituted into Eq. (18), and the resulting equation is solved for the flow rate in terms of the heat load and fluid temperature, the following equation for the thermal performance is generated:

$$\dot{m} = -76.24 \ln \left[5.0 \left(\frac{-R_{cw}\dot{Q} - R_{jc}\dot{Q} - 2.25 - 0.20\dot{Q} + T_j - T_f}{\dot{Q}} \right) \right] \quad (19)$$

IF $\dot{m}_{measured} \leq 0.0$: THEN $\dot{m}_{actual} = 0.0$
 ELSE $\dot{m}_{actual} = \dot{m}_{measured}$

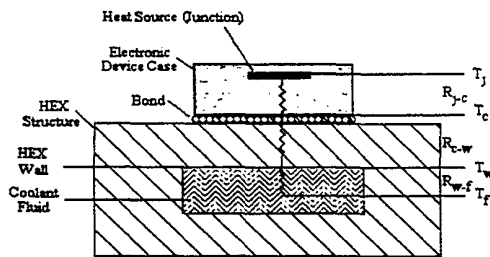


Figure 9. Thermal resistance and junction temperature placement.

For this case study's thermal performance equation, a logical expression must be inserted because the equation itself does not discern positive and negative values of the mass flow rate. The need for this logical expression results from the equation producing a heat flux capability for the HFHE at zero mass flow rate. When a stagnant flow exists and a heat flux is applied to the HFHE, the coolant temperature in the HFHE will increase. However, the thermal performance equation for the HFHE is based on the assumption that the coolant temperature is constant. Therefore, the condition of stagnant flow invalidates the thermal performance equation. The reason for this error is that the equation assumes a constant coolant temperature.

Therefore, an asymptote must be added to the thermal performance equation. This asymptote is the logical expression. The logical expression itself indicates that any negative values for the flow rate resulting from the input parameters in Eq. (19) in actuality mean that any positive non-zero flow through the HFHE is sufficient to remove the inputted heat flux. Furthermore, a positive value for the mass flow rate resulting from the input parameters in Eq. (19) reflects the actual minimum mass flow rate necessary to remove the given heat flux.

For this case study a family of curves were generated using Eq. (19) for the minimum mass flow rate required for the removal of a given heat flux as a function of the coolant temperature. However, because the thermal performance is dependent on the outside parameters of the thermal resistances, the thermal performance curves are presented over a range of possible thermal resistances. Figures 10, 11, and 12 represent the thermal performance for thermal resistances of 0.15, 0.20, and 0.25°C/(W/cm²), respectively. These curves represent the minimum mass flow rate necessary to remove the given heat flux for a given coolant temperature. As these plots show, for the lower heat loads (less than 20 W), the necessary mass flow rate is independent of the coolant temperature. For example, for thermal resistances of 0.20°C/(W/cm²), if the coolant temperature is below 348 K (75°C), then any flow rate through the HFHE is sufficient to remove a heat flux of 20 W/cm². However, as the heat load is increased, the necessary mass flow rate becomes dependent on the coolant temperature. For example, to remove a heat flux of 100 W/cm² with thermal resistances of 0.20°C/(W/cm²), the minimum necessary mass flow rate is 150 kg/hr at a coolant temperature of 298 K (25°C). However, if the coolant temperature is reduced to 290 K (17°C), then the minimum necessary mass flow rate through the HFHE reduces to 50 kg/hr. Furthermore, if the coolant temperature is reduced below 281 K (8°C), then any mass flow rate through the HFHE will remove 100 W/cm².

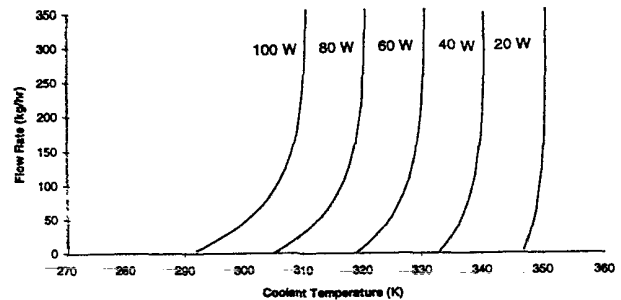


Figure 10. Thermal performance as a function of the heat load with $T_j = 363$ K and thermal resistances of 0.15°C/(W/cm²).

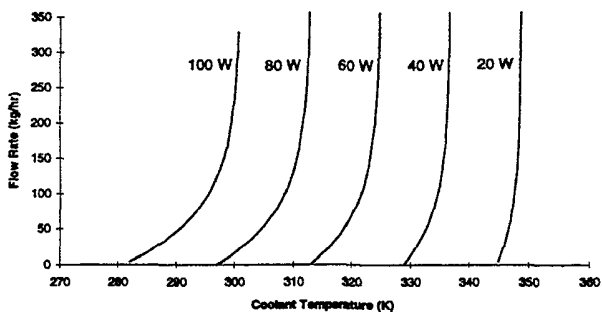


Figure 11. Thermal performance as a function of the heat load with $T_j = 363$ K and thermal resistances of $0.20^\circ\text{C}/(\text{W}/\text{cm}^2)$.

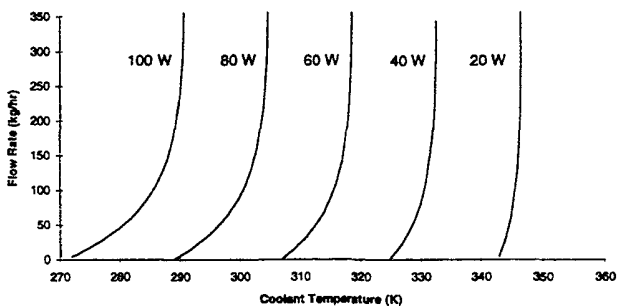


Figure 12. Thermal performance as a function of the heat load with $T_j = 363$ K and thermal resistances of $0.25^\circ\text{C}/(\text{W}/\text{cm}^2)$.

A further comparison between the various heat exchangers includes the maximum possible coolant temperature for the removal of a given heat flux. For this case study, a typical example of this type of comparison can be seen in Fig. 11, in which the flow rate necessary to generate a maximum cooling rate of 100 W per CHIC remains small until the inlet temperature approaches a value of 301 K. At this temperature the minimum flow rate necessary for a cooling rate of 100 W per CHIC increases to infinity. The maximum possible coolant temperature can be increased from 301 K by decreasing the thermal resistance of R_{jc} and R_{cw} . If the thermal resistance was reduced from 0.20 to $0.15^\circ\text{C}/(\text{W}/\text{cm}^2)$, the corresponding maximum possible coolant temperature is increased from 301 to 311 K.

Finally, a comparison between the various heat exchangers can be made on the dependency of the minimum flow rate on the thermal resistances. For this case study, the dependency can be seen in Figs. 10 through 12. As can be seen, an increase in thermal

resistances for both the case-to-wall and the case-to-junction of $0.05^\circ\text{C}/(\text{W}/\text{cm}^2)$ translates to a 10 K decrease in the maximum allowable coolant temperature for the applied heat flux of $100\text{ W}/\text{cm}^2$. While the $0.05^\circ\text{C}/(\text{W}/\text{cm}^2)$ increase in thermal resistances translates to a 2 K decrease in the maximum allowable coolant temperature for the applied heat flux of $20\text{ W}/\text{cm}^2$.

Maximum Heat Flux Capability

The last standard for the comparison between the heat exchangers is the maximum heat flux capability. For the case study of the HFHE, the operating conditions consist of a junction temperature of 90°C , a coolant temperature of 0°C , and a maximum pressure drop of 311 kPa. Using Eq. (10), this coolant temperature and pressure drop results in a mass flow rate of 182 kg/hr. Using this mass flow rate and the operating conditions, with a typical value for the thermal resistances between the wall and case and between the case and junction of $0.20^\circ\text{C}/(\text{W}/\text{cm}^2)$, the maximum heat flux can be calculated using Eq. (19). This maximum heat flux was calculated to be $142\text{ W}/\text{cm}^2$. However, the maximum heat flux capability is not a function solely dependent on the heat exchanger but on the thermal resistances and the coolant temperature, as shown in Eq. (19). These dependencies can be seen in Figs. 13 and 14.

Conclusions

Once the three standards for the heat exchanger, the hydraulic performance equation, thermal performance equation, and maximum heat flux capability, have been constructed, the various heat exchangers can be compared. This comparison should include an analysis similar to the following for the case study of the High Flux Heat Exchanger. For the operating conditions of a pressure drop of 311 kPa, a junction temperature of 363 K (90°C), thermal resistances of $0.20^\circ\text{C}/(\text{W}/\text{cm}^2)$, and a coolant temperature of 273 K (0°C), the maximum heat flux capability of the heat exchange is $142\text{ W}/\text{cm}^2$. However, the HFHE is not capable of removing $100\text{ W}/\text{cm}^2$ as the coolant temperature is increased past 301°C (28 K). In addition, to achieve the $142\text{ W}/\text{cm}^2$, a mass flow rate of 188 kg/hr is required. For the hydraulic performance equation, comparisons between heat exchangers can be made on the dependency of the mass flow rate on the pressure drop. In general, the HFHE is expected to contain a higher pressure drop for a given mass flow rate due to the abrupt turning of fluid flow through the orifice/spacer plates in each CHIC. The dependency of the coolant temperature on the pressure drop is a function of the coolant used and not related to the heat exchanger. For the thermal performance equation, comparisons between heat

exchangers can be made on the minimum flow rate required for the cooling a given heat flux. In addition, a further comparison between heat exchangers can be made on the range of possible coolant temperatures that can be used for the removal of a give heat flux. Finally, the most important comparison can be made on the maximum heat flux capability.

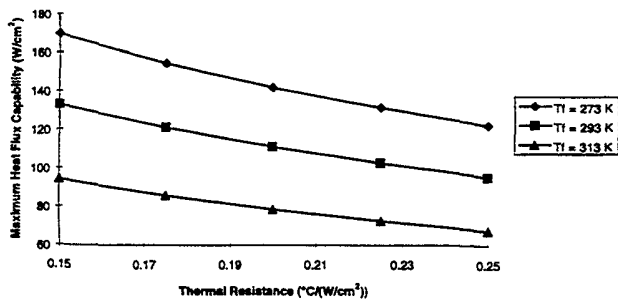


Figure 13. Maximum heat flux capability as a function of the thermal resistance and fluid temperature ($T_j = 363 \text{ K}$, $\Delta P = 311 \text{ kPa}$).

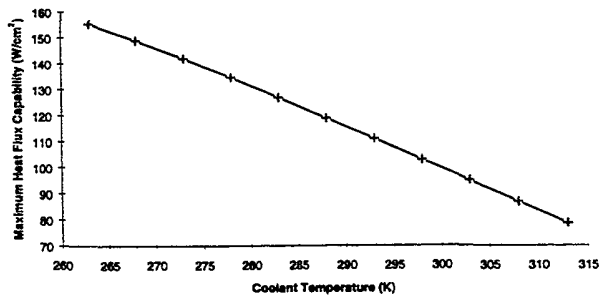


Figure 14. Maximum heat flux capability as a function of the thermal resistance and fluid temperature ($T_j = 363 \text{ K}$, $\Delta P = 311 \text{ kPa}$ and R_{cw} and $R_{jc} = 0.20^\circ\text{C}/(\text{W}/\text{cm}^2)$).

Acknowledgment

This research was conducted under sponsorship of the Air Force Wright Laboratory, Aero Propulsion and Power Directorate, Wright Patterson AFB, Ohio, with Dr. Jerry E. Beam and Dr. John E. Leland as Project Managers.

References

¹Mackowski, M. J., "Requirements for High Flux Cooling of Future Avionics Systems," SAE Paper No. 912104, September 1991.

²Flynn, E. M., "Evaluation of Cooling Concepts for High Power Avionics Applications," SAE Paper No. 921942, October 1992.

³Bland, T. J., Niggemann, R. E., and Parekh, M. B., "A Compact High Intensity Cooler (CHIC)," SAE Paper No. 831127, July 1983.

⁴Flynn, E. M., Downing, R. S., and Nguyen, D. C., "High Flux Heat Exchanger," Wright Laboratory Final Report No. WL-TR-94-2043, February 1994.

⁵Bland, T. J., Ciaccio, M. P., Downing, R. S., and Smith, W.G., "The Development of Advanced Cooling Methods for High-Power Electronics," SAE Paper No. 901962, October 1990.

⁶Grote, M. G., Hendron, R. E., Kipp, H. W., and Lapinski, J. R., "Test Results of Wafer Thin Coolers at Heat Fluxes from 5 to 125 W/cm²," SAE Paper No. 880997, July 1988.

⁷Flynn, E. M., and Mackowski, M. J., "High Flux Heat Exchanger," Wright Laboratory Interim Report No. WL-TR-93-2027, January 1993.

⁸Gschwender, L. J., Snyder, C. E., and Conte, A. A., "Polyalphaolefins as Candidate Replacements for Silicate Ester Dielectric Coolants in Military Applications," *Lubrication Engineering Journal*, Vol. 41, No. 4, pp. 221-228, April 1985.

⁹Zoppoth, R. C., and Dillard, J., "PAO Report: Extended Testing of Polyalphaolefins as a Dielectric/Coolant Fluid," Texas Instruments, Defense Systems and Electronics Group, Dallas, Tx, July 1988.

¹⁰Ghajar, A. J., "Comparison of Hydraulic and Thermal Performances of PAO and Coolanol 25R Liquid Coolants," Final Report, Summer Faculty Research Program, Wright Laboratory, August 1993.

¹¹Ghajar, A. J., Tang, W. C., and Beam, J. E., "Methodology for Comparison of Hydraulic and Thermal Performance of Alternative Heat Transfer Fluids in Complex Systems," *Heat Transfer Engineering*, Vol. 16, No. 1, pp. 68-72, 1995.